NANO LETTERS

2008
Vol. 8, No. 3
805-809

Spin Diode Based on Fe/MgO Double Tunnel Junction

A. Iovan,[†] S. Andersson,[†] Yu. G. Naidyuk,[†,‡] A. Vedyaev,[§] B. Dieny,[△] and V. Korenivski*,[†]

Nanostructure Physics, Royal Institute of Technology, 10691 Stockholm, Sweden, Department of Physics, Lomonosov State University, Moscow 119699, Russia, and SPINTEC, URA CEA/CNRS, Grenoble, France

Received October 17, 2007; Revised Manuscript Received January 20, 2008

ABSTRACT

We demonstrate a spin diode consisting of a semiconductor-free nanoscale Fe/MgO-based double tunnel junction. The device exhibits a near perfect spin-valve effect combined with a strong diode effect. The mechanism consistent with our data is resonant tunneling through discrete states in the middle ferromagnetic layer sandwiched by tunnel barriers of different spin-dependent transparency. The observed magnetoresistance is a record high >1000%, essentially making the structure an on/off spin switch. This, combined with the strong diode effect, ~100, demonstrates a new device principle, promising for memory and reprogrammable logic applications.

Discoveries of spin valves and magnetic tunnel junctions have inspired numerous sensor and memory applications.[1–5] Large magnetoresistance obtained in these devices motivates the great current research effort on developing spin-based diodes and transistors.[6] Implementing these magnetic logic elements in semiconductors is challenging, however, due to such fundamental issues as efficient spin injection and ferromagnetism at room temperature.[7–10] Double tunnel junctions (DTJs) having the two tunnel barriers of different transparency are expected to exhibit highly asymmetric conduction for different polarity bias, i.e., act as a current rectifier or a diode.[11] Such current rectification has been observed in double tunnel junctions[12,13] for the case of *spin-independent* conductivity (i.e., vanishing magneto-resistance, MR $\approx$ 0). Current rectification and MR have also been observed for *single* asymmetric tunnel barriers[14] however with limited rectification ratios (RR $\sim$ 10). Effects of resonant transmission have been recently demonstrated for Fe/MgO/Fe/MgO/Fe symmetric-tunnel-barrier DTJs[15] with only weak current rectification (RR $\sim$ 1). We have recently demonstrated a very strong diode effect (RR $\sim 10^4$) in asymmetric metal/oxide DTJs.[16] In this report we demonstrate a record high resonant tunneling MR (RTMR $\approx$ 4000%) combined with a high RR ($\sim$100) for an asymmetric magnetic DTJ, making the device an efficient hybrid of a spin switch and a diode. The material system we use in this demonstration is MgO-based magnetic tunnel junctions, where MR values 100–600% have been reported recently.[17–20]

F1/I1/F2/I2/N samples of structure Si/SiO/Fe(50 nm)/MgO(3 nm)/Fe(1–2 nm)/MgO(2–3 nm)/Au(30 nm) were deposited using dc magnetron sputtering at the base pressure of 1.3×10^{-8} mbar. The argon pressure of 4.0×10^{-3} mbar was used for deposition of the Fe layers. The magnesium oxide was reactively sputtered by adding 4.0×10^{-4} mbar of oxygen to the Ar sputter gas during the deposition of Mg. The different thickness of the MgO layers is responsible for the asymmetry in the transparency of the two tunnel barriers sandwiching the middle Fe layer. The nanometer thin middle Fe insulated by MgO from the outer electrodes is designed to have the thickness comparable to the electron Fermi wavelength in the material, resulting in the level spacing of the order of 100 meV. The stacks were patterned into nanopillars using a 150 nm ZEP520A positive resist. The resist was spun on to the multilayer samples and hardened by baking. A rectangular matrix of lines was drawn by e-beam lithography in the resist, which was subsequently developed to serve as a hard mask. This hard mask was then transferred in to TJ stacks using Ar ion beam etching. The nanopillar fabrication process was finalized by removing the resist mask with oxygen plasma. The resulting structure is a large array of DTJ vertical stacks, separated by trenches etched through the top Au electrode, the top MgO barrier, and the middle Fe electrode, down to the bottom MgO layer. Since the etching rate of MgO is much lower than that of metals, we could reliably stop the ion etch at the thicker bottom MgO layer using proper etch rate calibrations. Thus, the patterned stack is capped with Au, which acts as the top

* Corresponding author. E-mail: vk@kth.se.
[†] Royal Institute of Technology.
[‡] Permanent address: ILTPE, Kharkov, Ukraine.
[§] Lomonosov State University.
[△] SPINTEC, URA CEA/CNRS.

10.1021/nl072676z CCC: $40.75
Published on Web 02/20/2008

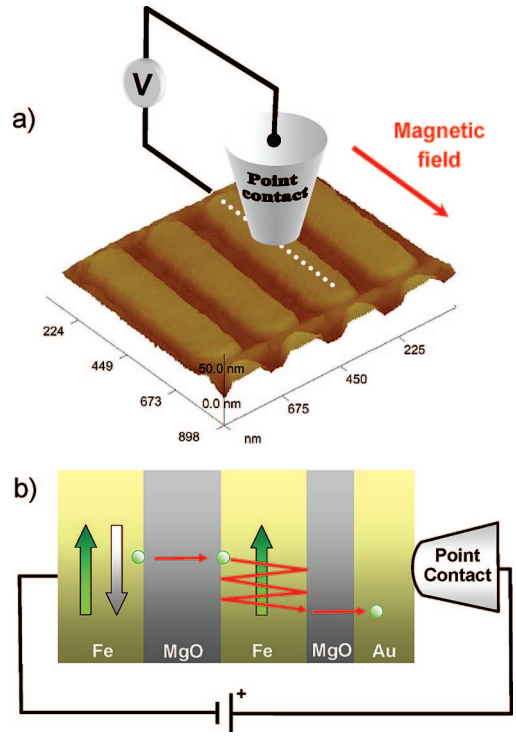

Figure 1. (a) STM image of an array of nanopillar junctions and schematic of the point-contact measurement technique. (b) Illustration of a magnetic double tunnel junction with a resonant transmission state in the middle quantum well.

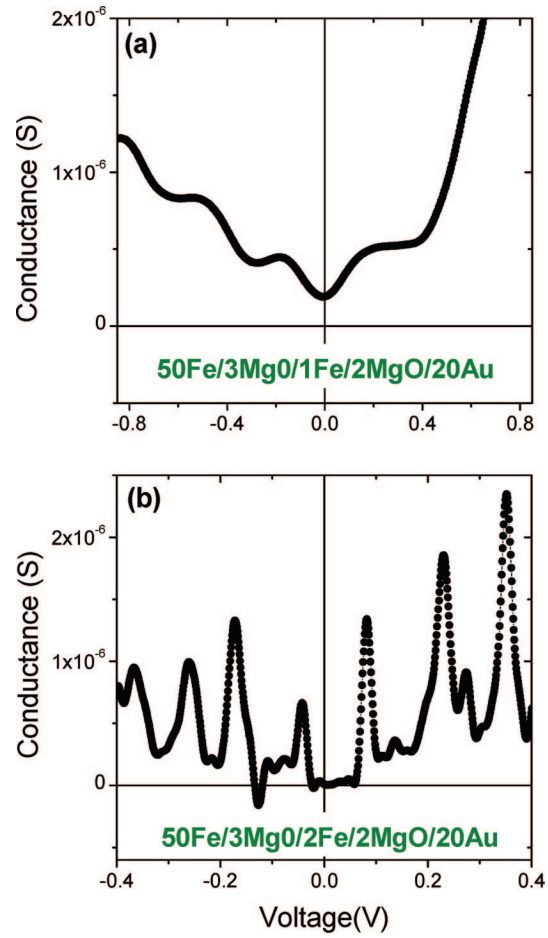

Figure 2. Differential conductance (dI/dV) as a function of bias voltage (V) for typical DTJs in the quantum transport regime. The numbers in the caption give the thickness of the individual layers in nanometers.

electrode of the DTJ and defines the lateral size of the junction. The lateral and vertical profiles of the samples were characterized using a scanning tunneling microscope (STM) at room temperature, as shown in Figure 1a. More details on the fabrication and STM characterization methods used in this study can be found elsewhere.[21] The thick Fe layer acts as the common bottom electrode for the DTJ array as a whole. The main advantage of this patterning process, with the etch stopped at the bottom MgO barrier, is that it minimizes shortcuts at the TJ perimeter due to possible redeposition compared to the case where the whole stack is patterned. By controlling the in-plane geometry of the nanopillars, we control the shape anisotropy of the middle Fe layer, which allows us to reliably separate the switching fields of the magnetically softer continuous bottom Fe layer and the magnetically harder patterned middle Fe layer.

The samples were measured using the point contact technique[22–24] directly in liquid helium (T = 4.2 K). This technique is based on mechanical micropositioning (rather than STM-like piezo-positioning) and allows spectroscopic transport measurements by establishing stable mechanical contacts of typical size ~10 nm, much smaller than the nanopillar size. The resistance of such point contacts is typically 1−10 Ω, negligible on the scale of the TJ resistance. The advantage of using such a nanomechanical technique is that possible damage to the sensitive regions of the DTJ from fabrication of the top contact is avoided, and a large number of stacks can be screened for a given sample in the same cool down. The stability of the contacts that were subsequently analyzed for quantum transport was verified by repeating the current–voltage and resistance-field sweeps several times for a given contact/stack.

The direct evidence of a coherent DTJ behavior, with the current flowing through discrete quantum well states in the center Fe electrode, is the measured conductance for two asymmetric DTJs, shown in Figure 2. The steps in current versus bias voltage (not shown) and the associated peaks in the differential conductance are spaced by 100–300 mV. The spacing decreases approximately inversely with the thickness of the middle Fe layer. This behavior is consistent with the data and the resonant conduction model of ref 15, including the broadening of the conduction peaks due to likely clustering of very thin Fe layers (1 nm). We therefore conclude that the observed conductance is due to resonant electron transport through discrete states in the middle layer, separated from the outer electrodes by two tunnel barriers.

Since the probability of tunneling decreases exponentially with the thickness of the tunnel barrier, the two tunnel barriers used (3 and 2 nm thick) in two of our DTJ samples have substantially different transparency. In this case of asymmetric barriers, theory predicts[11] asymmetric conduction for different polarity bias. We indeed observe pronounced transport asymmetry, with the rectification ratio RR =

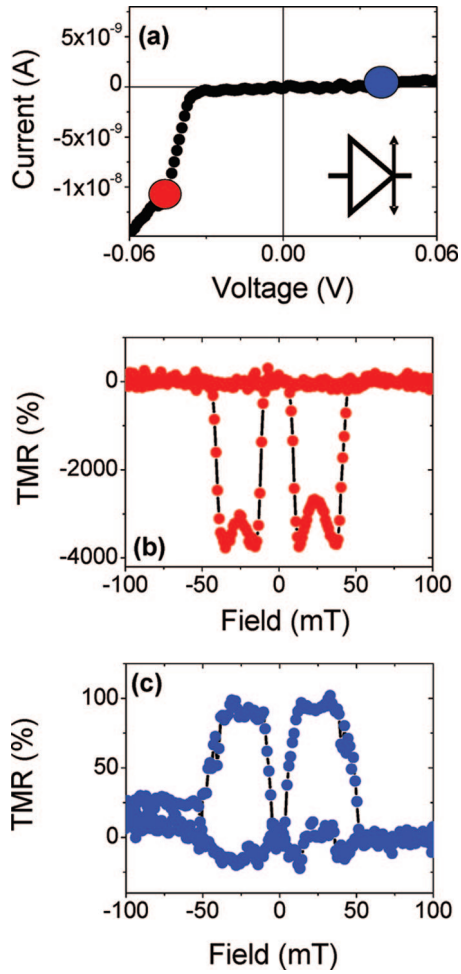

Figure 3. (a) Asymmetric current–voltage characteristics of a double tunnel junction in antiparallel magnetic state, exhibiting a strong diode effect. Magnetoresistance for a negative bias of −50 mV (b) and a positive bias of 40 mV (c). The inset to (a) shows a proposed circuit symbol for the device.

$|I(+V_b)/I(-V_b)|$ of up to 100 at $V_b < 100$ mV, shown in Figure 3a. This demonstrates a strong diode effect for a magnetic double tunnel junction.

All four samples fabricated, three DTJ samples and one single TJ control sample, showed a dependence of the resistance on the applied magnetic field, which is a good indication of the quality of the bottom MgO barrier and the patterning processes as a whole. One of the DTJ samples had a 2 nm thick Fe middle layer and symmetric, 3 nm thick MgO tunnel barriers. No $I-V$ asymmetry was observed for this symmetric DTJ sample (RR ∼ 1, ∼10 contacts with symmetric $I-V$ values measured). On the other hand, pronounced $I-V$ asymmetry was observed for two *asymmetric* DTJ samples having 1 and 2 nm thick middle Fe layer (such as shown Figure 2). For these two samples, the tunnel barrier thickness was 3 nm for the bottom MgO layer and 2 nm for the top MgO layer. Five contacts showed resonant conductance peaks combined with $I-V$ asymmetry. Four contacts showed MR combined with resonant conductance. Two contacts (2 nm thick middle Fe) showed an inverted (negative) MR. One of the contacts (PC7: 50 Fe/3 MgO/2 Fe/2 MgO/20 Au) showed very pronounced resonant features (Figure 2b), which greatly amplified the MR at low bias. This contact was studied in detail in terms of the $I-V$ and MR beahvior (∼25 $I-V$ sweeps and ∼20 $R-H$ sweeps performed over 2 days, before the contact was lost at high bias). A representative set of these magneto-transport data is discussed below, where the MR was obtained from R vs H field sweeps.

The magnetoresistance at a positive bias of 40 mV shown in Figure 3c exhibits the behavior typical of spin valves: the conductance is high at high fields where the magnetizations of the Fe layers are parallel, and low at intermediate fields where the magnetizations are antiparallel. Interestingly, reversing the bias direction results in an inverted magnetoresistance, as shown in Figure 3b for $V_b = -50$ mV. The switching fields of ∼4 and ∼40 mT are the same as those for the positive bias configuration. The lower switching field corresponds to the reversal of the magnetization of the unpatterned bottom Fe layer. The higher switching field corresponds to the reversal of the magnetization in the middle Fe electrode and is consistent in magnitude with the shape anisotropy field due to the in-plane patterning (170 × 800 nm^2 in this case). The fact that the switching of the middle electrode is sharp is additional evidence that the thin Fe layer is continuous, since nanogranular Fe would saturate in much higher fields (∼1 T for spherical particles) over a much broader field range (0−1 T). Thus, for negative bias, near the first negative conductance resonance (see Figure 2b), the conductivity is low at high fields where the magnetizations are parallel and high at intermediate fields where the magnetizations are antiparallel. The associated MR is negative and approaches 4000%, as shown in Figure 3b.

Our test samples with single tunnel barriers universally show a positive MR as expected for spin valves.[25,26] Thus, the inverted MR is the signature of the magnetic DTJ, which is in the quantum transport regime (see Figure 2). This behavior can originate from the spin dependence of the quantized energy states in the middle electrode.[27] It has been predicted that such discrete states can shift as a function of the magnetic misalignment of the two ferromagnetic electrodes.[28–30] Our interpretation of the observed MR behavior is as follows.

As shown in Figure 2, the conductance through the DTJ exhibits multiple peaks as a function of voltage. This behavior is expected for electron transmission through discrete quantum well states (QWSs), with the current in the general case given by

$$J_{\uparrow} = \frac{e}{2\pi\hbar}\int_{\mu_0}^{\mu_0+eV} dE \sum_n \frac{\Gamma^n_{L\uparrow}\cdot\Gamma^n_{R\uparrow(\downarrow)}}{(E_n-E)^2+(\Gamma^n_{L\uparrow}+\Gamma^n_{R\uparrow(\downarrow)})^2} \qquad (1)$$

Here $J_{\uparrow}$ is the spin-up current component, with the electrons transmitted through QWSs of energy E_n and width Γ^n. The widths of the resonant levels E_n are proportional to the respective transmissivities, $\Gamma^n \sim T_{L,R}$, which for magnetic tunnel junctions are spin dependent. The transmissivities are in turn exponential functions of the respective tunnel barrier thickness.[31] V is the bias voltage applied to the DTJ, and μ_0 is the chemical potential in the outer electrodes at zero bias. Indeed, at sufficiently low temperature the resonant terms

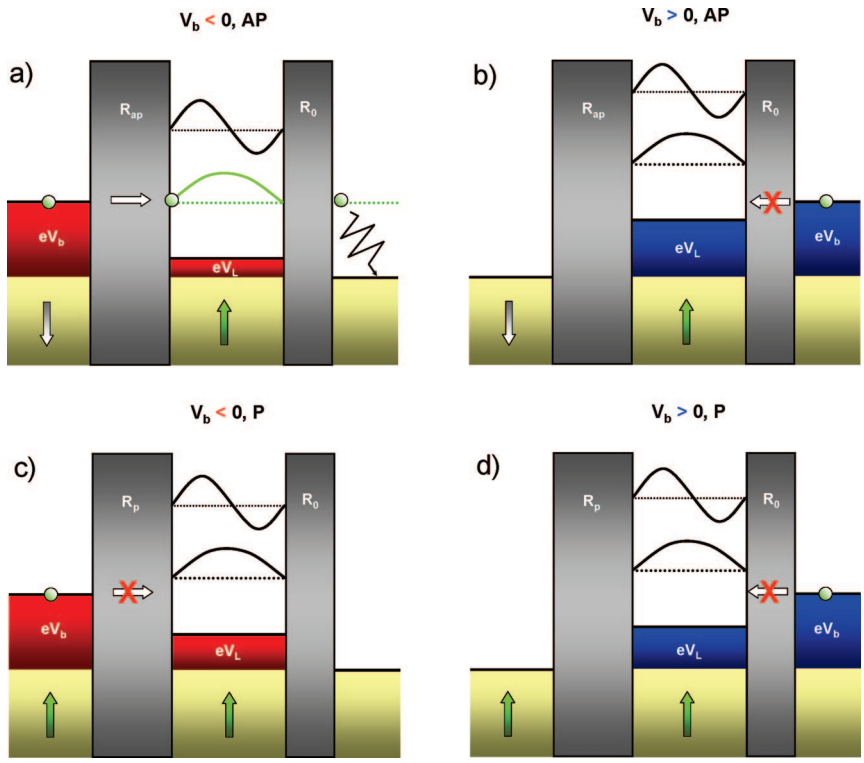

Figure 4. Spin-dependent energy diagram of the DTJ: (a) negative bias, antiparallel magnetic state; (b) positive bias, antiparallel state; (c) negative bias, parallel magnetic state; (d) positive bias, parallel magnetic state. The bias voltage across the left spin-dependent junction is a function the bias polarity, DTJ asymmetry, and the magnetic state of the left junction and is generally different for the four configurations of (a−c). Only configuration (a) corresponds to resonant transmission through one of the discrete states in the middle electrode.

in eq 1 integrated over all available electron energies produce steplike $I-V$ characteristics and hence resonant peaks in the differential conductance of the kind we observe experimentally (Figure 2a,b).

To explain the observed magnetoresistance (Figure 3b,c), it will be sufficient to consider the qualitative energy diagram shown in Figure 4. Thus, Figure 4a depicts the antiparallel configuration, with the electrons flowing rightward from Fe to Au, and the bias voltage taken to match one of the QW states. The electron transmission is resonant, resulting in a high conductance in this case. Upon reversal of one of the magnetic electrodes into the parallel magnetic state of the left Fe/MgO/Fe junction, this junction resistance decreases as does the voltage drop across it. With the fixed bias voltage across the double junction, this leads to a shift of the energy levels in the middle electrode, as illustrated in Figure 4b, such that the transmission becomes off-resonant and the conductance of the DTJ as a whole decreases. This consideration explains the negative MR, which is the opposite of the normal spin-valve effect where the high conductance corresponds to the parallel magnetic configuration.

Reversing the polarity of the bias shifts the QW levels in the middle electrode such that the electron transmission is off-resonant for both magnetic states of the left junction, as illustrated in Figure 4c,d. Since the left MgO barrier is thicker, it is the left magnetic junction that contributes most to the total resistance of the DTJ. One therefore expects for this bias configuration a TMR of type normal for Fe/MgO/Fe single junctions, which is indeed observed—the conduction is high for the parallel magnetic state and low for the antiparallel state.

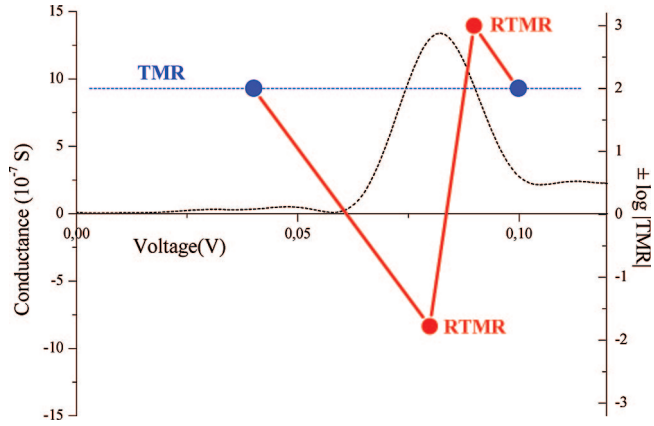

Figure 5. Conductance of Figure 2b for low positive bias (dashed line, left axis). MR of the DTJ at four fixed bias points near the first resonance peak (blue and red dots, corresponding to conventional TMR and resonant TMR, respectively).

As expected for a nonresonant transmission, the magnitude of the measured positive MR corresponds well with the values reported for Fe/MgO/Fe single junctions of 100–600%. The observed negative, resonant MR on the other hand is an order of magnitude higher. This substantial difference in magnitude in addition to the difference in sign of the observed MR provides an important additional confirmation of our interpretation of the observed magnetoconductance effect as due to resonant spin-dependent tunneling through quantum well states of the F/F/N double tunnel junction.

To additionally strengthen our interpretation in terms of spin resonant tunneling through the magnetic DTJ, we show in Figure 5 the bias dependence of the MR for the first *positive* resonance peak observed at +80 mV. Off-resonance, below ~60 mV, the DTJ exhibits the conventional positive TMR of ~100% (log |TMR| ≈ 2, same as in Figure 3c), corresponding to the TMR of the left tunnel junction in our case. As the bias is increased to 80 mV, the MR changes sign (shown in the figure as −log |TMR| ≈ −2). A further increase in bias to 90 mV leads to another sign change in the MR, which now is positive and significantly enhanced over the conventional value, RTMR ~1000%, since the bias is still near-resonance. Further increase of the bias brings the MR to the conventional, off-resonance value (~100% in our case). This oscillating in sign, resonant tunneling magnetoresistance (RTMR) is in excellent agreement with the spin-dependent resonant transmission model described in Figure 4, which predicts an enhanced, sign-changing MR near a conductance peak.

In conclusion, the measured magnetoresistance is record high, essentially making the structure an on/off spin switch. This, combined with the strong diode effect, demonstrates a new device principle, promising for memory and reprogrammable logic applications.

References

(1) Baibich, M. N.; Broto, J. M.; Fert, A.; Van Dau Nguyen, F.; Petroff, F.; Etienne, P.; Creuzet, G.; Friederich, A.; Chazelas, J. *Phys. Rev. Lett.* **1988**, *61*, 2472.
(2) Dieny, B.; Speriosu, V. S.; Parkin, S. S. P.; Gurney, B. A.; Wilhoit, D. R.; Mauri, D. *Phys. Rev. B* **1991**, *43*, 1297.
(3) Moodera, J. S.; Kinder, L. R.; Wong, T. M.; Meservey, R. *Phys. Rev. Lett.* **1995**, *74*, 3273.
(4) Miyazaki, T.; Tezuka, N. *J. Magn. Magn. Mater.* **1995**, *139*, L231.
(5) Parkin, S. P. P. *J. Appl. Phys.* **1999**, *85*, 5828.
(6) Zutic, I.; Fabian, J.; Das Sarma, S. *Rev. Mod. Phys.* **2004**, *76*, 323.
(7) Schmidt, G.; Ferrand, D.; Molenkamp, L. W.; Filip, A. T.; van Wees, B. J. *Phys. Rev. B* **2000**, *62*, R4790.
(8) Ohno, H. *Science* **1998**, *281*, 951.
(9) Ohno, H.; Chiba, D.; Matsukura, F.; Omiya, T.; Abe, E.; Dietl, T.; Ohno, Y.; Otani, K. *Nature* **2000**, *408*, 944.
(10) Park, Y. D.; Hanbicki, A. T.; Erwin, S. C.; Hellberg, C. S.; Sullivan, M.; Mattson, J. E.; Ambrose, T. F.; Spanos, Wilson, G.; Jonker, B. T. *Science* **2002**, *295*, 651.
(11) Chshiev, M.; Stoeffler, D.; Vedyayev, A.; Ounadjela, K. *Europhys. Lett.* **2002**, *58*, 257–263.
(12) Tiusan, C.; Chshiev, M.; Iovan, A.; da Costa, V.; Stoeffler, D.; Dimopoulos, T.; Ounadjela, K. *Appl. Phys. Lett.* **2001**, *79*, 4231.
(13) Iovan A. *PhD thesis* IPCMS, Strasbourg, September 2004.
(14) de Buttet, C.; Hehn, M.; Montaigne, F.; Tiusan, C.; Malinowski, G.; Schuhl, A.; Snoeck, E.; Zoll, S. *Phys. Rev. B* **2006**, *73*, 104439.
(15) Nozaki, T.; Tezuka, N.; Inomata, K. *Phys. Rev. Lett.* **2006**, *96*, 027208.
(16) Iovan, A.; Haviland, D. B.; Korenivski, V. *Appl. Phys. Lett.* **2006**, *88*, 163503.
(17) Butler, W. H.; Zhang, X.-G.; Schulthess, T. C.; MacLaren, J. M. *Phys. Rev. B* **2001**, *63*, 054416.
(18) Parkin, S. S.P.; Kaiser, C.; Panchula, A.; Rice, P. M.; Hughes, B.; Samant, M.; Yang, S. H. *Nat. Mater.* **2004**, *3*, 862.
(19) Yuasa, S.; Nagahama, T.; Fukushima, A.; Suzuki, Y.; Ando, K. *Nat. Mater.* **2004**, *3*, 868.
(20) Yuasa, S.; Fukushima, A.; Kubota, H.; Suzuki, Y.; Ando, K. *Appl. Phys. Lett.* **2006**, *89*, 042505.
(21) Iovan, A.; Lam, K.; Andersson, S.; Cherepov, S. S.; Haviland, D. B.; Korenivski, V. *IEEE Trans. Magn.* **2007**, *43*, 2818.
(22) Naidyuk, Yu. G.; Yanson, I. K. *Point-Contact Spectroscopy*; Springer Series in Solid-State Sciences, 145; Springer Science+Business Media, Inc.: New York, 2005.
(23) Yanson, I. K.; Naidyuk, Yu.G.; Bashlakov, D. L.; Fisun, V. V.; Balkashin, O. P.; Korenivski, V.; Konovalenko, A.; Shekhter, R. I. *Phys. Rev. Lett.* **2005**, *95*, 186602.
(24) Yanson, I. K.; Naidyuk, Yu. G.; Fisun, V. V.; Konovalenko, A.; Balkashin, O. P.; Yu, L.; Korenivski, V. *Nano Lett.* **2007**, *7*, 927.
(25) Julliere, M. *Phys. Lett. A* **1975**, *54*, 225.
(26) Slonczewski, J. C. *Phys. Rev. B* **1989**, *39*, 6995.
(27) Yakushiji, K.; Ernult, F.; Imamura, H.; Yamane, K.; Mitani, S.; Takanashi, K.; Takahashi, S.; Maekawa, S.; Fujimori, H. *Nat. Mater.* **2005**, *4*, 57.
(28) Barnas, J.; Fert, A. *Phys. Rev. Lett.* **2005**, *80*, 1058.
(29) Brataas, A.; Nazarov, Y. V.; Inoue, J.; Bauer, G. E. W. *Phys. Rev. B* **1999**, *59*, 93.
(30) Barnas, J.; Fert, A. *Europhys. Lett.* **1998**, *44*, 85–90.
(31) Ferry, D. K.; Goodnick, S. M. *Transport in Nanostructures*; Cambridge University Press: Cambridge, 1997.

NL072676Z